Journal of Zhejiang University-SCIENCE A (Applied Physics & Engineering)
ISSN 1673-565X (Print); ISSN 1862-1775 (Online)
www.zju.edu.cn/jzus; www.springerlink.com
E-mail: jzus@zju.edu.cn

Analytical model for straight hemming based on minimum energy method*

Qian WANG, Xiang-huai DONG†‡, He-zong LI, Hai-ming ZHANG

(*National Engineering Research Center of Die & Mold CAD, Shanghai Jiao Tong University, Shanghai 200030, China*)

†E-mail: dongxh@sjtu.edu.cn

Received Nov. 3, 2010; Revision accepted Feb. 22, 2011; Crosschecked June 21, 2011

Abstract: An analytical model for straight hemming was developed based on minimum energy method to study the effect of flanging die corner radius on hemming qualities. In order to calculate plastic strain and strain energy more exactly, the neutral layer of specimen corner after hemming is assumed to be a half ellipse with its major semi-axis unknown. Isotropic hardening rule is adopted to describe bending and reverse bending processes neglecting Bauschinger effect. The model takes into account the material property parameters in order to satisfy a wide application range of different materials. Specimen profile, creepage/growing (roll-in/roll-out) and maximum equivalent strain are predicted, which are greatly influenced by the flanging die corner radius. Experimental facilities were designed and hemming experiments were undertaken. The predicted results of the present analytical model were compared to experimental data as well as finite element (FE) simulation results. It was confirmed that they are in good agreement, and the model can be used to evaluate whether the material used as an outer panel for hemming is appropriate and to optimize process parameters when the material used for hemming is changed.

Key words: Analytical model, Minimum energy method, Defects, Large deformation, Hemming
doi:10.1631/jzus.A1000458 **Document code:** A **CLC number:** TG301

1 Introduction

Hemming is often the last procedure in car stamping operations, and is used either to improve appearance or to attach one sheet metal part to another especially in the case of automotive panels such as doors, hoods, and deck-lids (Muderrisoglu *et al*., 1996). Hemming operations are usually undertaken in three steps to fold a flat sheet to 180°: flanging (90°), pre-hemming (135°), and final hemming (180°). The major quality problems related with hemming are creepage/growing, recoil and warp, and crack. Creepage/growing, and recoil and warp are surface defects, which are caused by lack of enough restraints, while crack usually occurs in materials of weak ductility.

In the past, researchers studied effects of process parameters, such as flanging die corner radius, punch-die clearance, pre-hemming punch path, and friction coefficient, on hemming through experiments and finite element (FE) simulations. Muderrisoglu *et al*. (1996) studied the effect of flanging die corner radius and flanging height on hemming operations such as punch load, springback, and bottom deflection. Based on the work of Muderrisoglu *et al*. (1996), more systematic work were undertaken to investigate the basics of hemming operations, and tool design modifications to improve hemming quality were made (Livatyali and Altan, 2001; Livatyali and Larris, 2004; Livatyali e*t al*., 2000; 2002; 2004). By using modified flat hems, required hemming dimensions are obtained. Zhang *et al*. (2000; 2001; 2003) investigated the mechanisms of occurrence of

‡ Corresponding author

* Project supported by the National Natural Science Foundation for Key Program of China (No. 50835002), the National Natural Science Foundation of China (No. 50975174), and the National Natural Science Foundation for Innovative Research Group of China (No. 50821003)

creepage/growing, recoil and warp, and proposed hemming process optimization using design and analysis of computer experimental methods. As a result of those researches, flanging die corner radius, pre-hemming path, and final hemming force are considered to be the most important parameters that affect hemming qualities. FE simulations are mainly concentrated on fracture and crack. Lin *et al*. (2009) introduced plane-strain tensile tests and a fracture criterion of maximum surface strain to evaluate formability of hemming of aluminum alloys. Maoût *et al*. (2009) adopted the critical void volume fraction in Gurson-Tvergaard-Needleman (GTN) model to determine the occurrence of crack in 6000 series of aluminum alloy hemming processes. Hu *et al*. (2010) proposed a ductile facture criterion for roller hemming limit of aluminum alloy 6061-T6.

There are few theoretical studies, most of which are concentrated on the first step of hemming-flanging. Buranathiti and Cao (2004) developed an effective analytical model to predict springback of a straight flanging process by conducting bending moment computation, and geometry and configuration calculation. Song *et al*. (2001) evaluated the prediction reliability of different methods for straight flanging operations. Wang *et al*. (1994; 1995) and Wang and Wenner (1974) presented two analytical models of introflexion/stretch and outcurve/shrink flanges. Hu *et al*. (2003) modified the models of Wang *et al*. (1994; 1995) and Wang and Wenner (1974), and established the calculation models of blank size on the condition of known flange height. However, the deformation of pre-hemming and final hemming are much more complicated than flanging. There is no related research on pre-hemming. By using a circular neutral layer assumption, Zhang (2001) first proposed an analytical model to calculate creepage based on pure geometrical assumption. Zhang (2001) claimed that the occurrence of creepage arises mainly from geometric constraints and the computation results showed that creepage is in proportion to thickness and flanging die radius. Zhang's model included no consideration of the material parameters. As a result, regardless of the kind of the material used, the value of creepage is maintained as a constant, which is not reasonable.

From the viewpoint of energy method, an analytical model for straight hemming was developed in this paper. The present study aims to predict deformation defects in hemming, which can help to evaluate whether or not the material of outer panel for hemming is appropriate and to optimize process parameters when the material is changed. It is also expected to be extended to 3D hemming with edge/surface curvature where FE analysis is very time consuming and is hard to reach convergence. Because of the uncertainty of boundary conditions and contact conditions during hemming deformation, specimen shape is very difficult to determine. With the observation of experiments and FE simulations, the neutral layer of the specimen corner at the end of hemming processes is assumed to be a half ellipse. To determine its major semi-axis, the minimum energy method is used based on the assumption that the true value of the major semi-axis will result in the minimum strain energy. By minimizing the energy function, which is described as the function of material parameters and process parameters, the unknown parameters can be obtained. As large deformation occurs during hemming, strain energy caused by elastic deformation can be ignored. Based on the above consideration, plastic strain field is calculated first. Then, equivalent plastic strain and stress are calculated to determine plastic strain energy. Finally, by solving the derived plastic strain energy equations, the value of semi-major axis is obtained. After the hemming profile is determined, hemming defects are predicted. Experiments and FE simulations are carried out using three different kinds of materials to verify the analytical model. As material parameters are introduced into strain energy, the method is appropriate for wide applications.

2 Analytical model

2.1 Geometrical model and assumption

Fig. 1 illustrates the geometry of the present analytical model. Deformation of pre-hemming is ignored for simplicity. A flat sheet as an outer panel is first flanged to the shape of Fig. 1a, and then is hemmed to the shape of Fig. 1b attaching to the inner panel. During flanging, the flat sheet is bent to a specified radius R_f as shown in Fig. 1a. Deformation is mainly concentrated in the corner. The strain field is easy to obtain by assuming that the corner is a quarter of a circle. In Fig. 1a, the neutral layer of $\overset{\frown}{Q_1Q_2}$ is a

circular arc; Point B is the midpoint of $\overset{\frown}{Q_1Q_2}$; Point N corresponds to the start point of where the inner panel is located on the outer panel, which is located beyond the arc according to industrial experience; D and D' are the endpoints of flange before and after flanging process. The flanged sheet inner radius is assumed to be the flanging die corner radius R_f. Corresponding locations of points Q_1, Q_2, and B on the outer surface are Q_{1O}, Q_{2O}, and B_O, respectively. Accordingly, the neutral layer's radius is $R_d=R_f+t/2$, where t is the sheet thickness. In hemming processes, because part of the outer panel is compressed by the inner panel and the corner of the outer panel deforms without sufficient constraints, the shape of the corner is difficult to determine.

In order to simplify the problem, a half ellipse is assumed to approximate the neutral layer profile after hemming. In Fig. 1b, the half ellipse is $\overset{\frown}{CA'}$. FE analysis results show that after hemming the midpoint of $\overset{\frown}{Q_1Q_2}$ is very close to that of $\overset{\frown}{CA'}$, so the two midpoints are assumed to be the same point B for simplicity. The lengths of ellipse's two semi-axis are a and b respectively. Assuming the inner panel has the same thickness as the outer panel, and thus the final hemming punch stroke ends at a position of three times of the sheet thickness, and the value of a is equal to the sheet thickness.

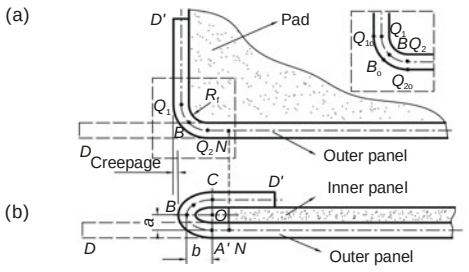

Fig. 1 Geometrical model of hemming
(a) Flanging; (b) Hemming

Basic assumptions of the theoretical calculation are as follows:

1. Neutral layer is located at the middle layer of the sheet during the whole processes.

2. Plane that is vertical to the neutral layer maintains a vertical plane.

3. Relationship between the equivalent strain $\bar{\varepsilon}$ and the equivalent stress $\bar{\sigma}$ is $\bar{\sigma}=\sigma_0+E_p\bar{\varepsilon}$, where σ_0 is the initial yield stress and E_p is the plastic hardening modulus.

4. Contribution of the elastic part of strain energy is ignored.

5. Specimen deforms under the plane strain condition.

2.2 Calculation of plastic strain and energy

2.2.1 Strain distribution in flanging and hemming

Specimen width is much greater than thickness; therefore, hemming process is considered as plane strain deformation. In the $o\zeta\theta$ plane of the flanging specimen as shown in Fig. 2, the radial strain $\varepsilon_{\zeta f}$ and circumferential strain $\varepsilon_{\theta f}$ can be written as

$$\varepsilon_{\theta f}=-\varepsilon_{\zeta f}=\ln\frac{(R_d+\zeta)\mathrm{d}\theta}{R_d\mathrm{d}\theta}=\ln\left(1+\frac{\zeta}{R_d}\right), \qquad (1)$$

where ζ and θ are the normal and tangential directions of the sheet, respectively, and f denotes the flanging stage.

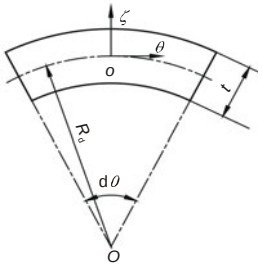

Fig. 2 Schematic of corner section

After hemming, the curvature of the neutral layer changes and is not a constant on different points of the semi-ellipse. R_d in Eq. (1) is replaced with ρ_n as a generalized (variable) curvature. The radius of curvature of the neutral layer $\overset{\frown}{CA'}$ after hemming is calculated using curvature formula as follows:

$$\rho_n=\frac{\sqrt{(1+y'^2)^3}}{|y''|}, \qquad (2)$$

where ρ_n is the curvature radius of the neutral layer,

and y' and y'' are the first and the second order derivatives of curve function y, respectively.

Parametrical function of ellipse is

$$\begin{cases} x = a\cos\theta, & 0 \le \theta \le \pi, \\ y = b\sin\theta, & 0 \le \theta \le \pi, \end{cases} \tag{3}$$

where θ is the eccentric anomaly. Then,

$$\begin{aligned} &\mathrm{d}x = -a\sin\theta\mathrm{d}\theta,\ \mathrm{d}y = b\cos\theta\mathrm{d}\theta, \\ &y' = -\frac{b\cos\theta}{a\sin\theta},\ y'' = -\frac{b}{a^2\sin^3\theta}. \end{aligned} \tag{4}$$

Substituting Eq. (4) into Eq. (2), we can obtain

$$\rho_{\mathrm{n}} = (b^2\cos^2\theta + a^2\sin^2\theta)\sqrt{\frac{\cos^2\theta}{a^2} + \frac{\sin^2\theta}{b^2}}, \tag{5}$$

where ρ_{n} is the radius of curvature of neutral layer $\widehat{CA'}$. Particularly,

$$\begin{cases} \rho_{\mathrm{n}A'} = \rho_{\mathrm{n}C} = b^2/a, \theta = 0, \pi, \\ \rho_{\mathrm{n}B} = a^2/b, \theta = \pi/2. \end{cases} \tag{6}$$

Thus, the circumferential strain increment from flanging to hemming can be calculated as

$$\Delta\varepsilon_\theta = \ln\frac{1+\zeta/\rho_{\mathrm{n}}}{1+\zeta/R_{\mathrm{d}}}. \tag{7}$$

Considering the deformation history of flanging to hemming, arc $\widehat{Q_1Q_2}$ may experience two different deformation processes as follows:

1. Loading process: After flanging, part of the arc will keep on loading, and its curvature keeps increasing ($\rho_{\mathrm{n}}<R_{\mathrm{d}}$). Thus, the absolute value of circumferential strain increases. For tension layer the tangential strain component $\Delta\varepsilon_{\theta 1}$ is positive, and for compression layer $\Delta\varepsilon_{\theta 1}$ is negative. Particularly, if the arc $\widehat{Q_1Q_2}$ is not long enough, part of the straight line ($R_{\mathrm{d}}\to\infty$) is bent to ρ_{n}:

$$\Delta\varepsilon_{\theta 1} = \ln\frac{1+\zeta/\rho_n}{1+\zeta/R_{\mathrm{d}}} = \ln(1+\zeta/\rho_n). \tag{8}$$

2. Reverse loading process: After flanging, part of the arc experiences reverse bending, and its curvature decreases ($\rho_{\mathrm{n}}>R_{\mathrm{d}}$). Thus, the absolute value of circumferential strain decreases. For tension layer the tangential strain component $\Delta\varepsilon_{\theta 2}$ is negative, and for compression layer $\Delta\varepsilon_{\theta 2}$ is positive. Particularly, part of the arc experiences reverse bending until being flattened, and its curvature decreases to zero ($\rho_{\mathrm{n}}\to\infty$):

$$\Delta\varepsilon_{\theta 2} = \ln\frac{1+\zeta/\rho_n}{1+\zeta/R_{\mathrm{d}}} = -\ln(1+\zeta/R_{\mathrm{d}}). \tag{9}$$

Taking the deformation process of $\widehat{BQ_1}$ in Fig. 1a as an example to help explain the two kinds of deformation processes and make clear how the flanging die corner radius affected the loading processes. Unlike a circle, the neutral layer curvature of an ellipse decreases from point B to point C in $\widehat{BC}$ as shown in Fig. 3. Suppose the curvature radius at point M is equal to the neutral layer curvature radius after flanging, that is, $\rho_{\mathrm{n}M}=R_{\mathrm{d}}=R_{\mathrm{f}}+t/2$. After hemming, if Q_1 lies in $\widehat{BM}$ as shown in Fig. 3a, $\widehat{BQ_1}$ in Fig. 1a has experienced loading process, and part of the straight zone Q_1D in Fig. 1a has experienced the particular loading process to become $\widehat{Q_1C}$. If Q_1 lies in $\widehat{MC}$ as shown in Fig. 3b, part of $\widehat{BQ_1}$ has experienced loading process to become $\widehat{BM}$, part of $\widehat{BQ_1}$ has experienced reverse loading process to become $\widehat{MQ_1}$ and part of the straight zone Q_1D in Fig. 1a has experienced the particular loading process to become $\widehat{Q_1C}$. Specifically, if the length of $\widehat{BQ_1}$ in Fig. 1a is long enough to make Q_1 lie in the straight zone CD' as shown in Fig. 3c, part of $\widehat{BQ_1}$ has experienced the

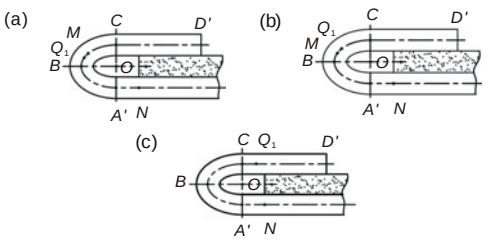

Fig. 3 Deformation modes
(a) Mode a; (b) Mode b; (c) Mode c

particular reverse loading process to become CQ_1. Because of the geometric symmetry, arc $\overset{\frown}{BQ_2}$ in Fig. 1a experiences the same deformation processes as arc $\overset{\frown}{BQ_1}$.

2.2.2 Calculation of strain energy and solution of the parameter *b*

As stress components are difficult to obtain, plastic strain energy is calculated through equivalent strain and equivalent stress:

$$W=\int\bar{\sigma}\Delta\bar{\varepsilon}\mathrm{d}V=\int\bar{\sigma}_k\Delta\bar{\varepsilon}_k\mathrm{d}\zeta\mathrm{d}s, \tag{10}$$

$$\begin{aligned}\int\mathrm{d}s&=\int\sqrt{(\mathrm{d}x)^2+(\mathrm{d}y)^2}\\&=\int\sqrt{a^2\sin^2\theta+b^2\cos^2\theta}\mathrm{d}\theta\\&=\int_{\varphi_{k-1}}^{\varphi_k}\sqrt{a^2\cos^2\varphi+b^2\sin^2\varphi}\mathrm{d}\varphi,\end{aligned} \tag{11}$$

where dV is the volume increment per unit width, and ds is the curve length increment. $\Delta\bar{\varepsilon}$ is the increment of equivalent plastic strain from Fig. 1a to Fig. 1b; subscript k indicates different deformed arcs under different loading processes; $\varphi=\theta-\pi/2$, φ_{k-1} and φ_k are the angles corresponding to the two end points of the deformed zones, and $-\pi/2\le\varphi_{k-1}<\varphi_k\le\pi/2$. Taking $\overset{\frown}{BC}$ in Fig. 3 as an example, $\varphi_B=0$, $\varphi_C=\pi/2$, φ_M can be obtained by solving Eq. (5) as $\rho_{nM}=R_d=R_f+t/2$ is known, and φ_{Q1} can be obtained through Eq. (11) as the curve length of $\overset{\frown}{BC}$ $s_{BC}=\pi R_d/4$ is known.

Under the assumption of plane strain condition: $\varepsilon_\theta=-\varepsilon_\zeta$, and $\varepsilon_z=0$, where ε_z is strain component along width direction, we can obtain

$$\Delta\bar{\varepsilon}_k=\frac{2\sqrt{3}}{3}\left|\Delta\varepsilon_{\theta k}\right|. \tag{12}$$

Isotropic hardening rule is introduced to describe reverse bending:

$$\bar{\sigma}_k=\sigma_0+E_p(\bar{\varepsilon}_{fk}+\Delta\bar{\varepsilon}_k), \tag{13}$$

where $\bar{\varepsilon}_f$ is the equivalent strain after flanging.

For simplicity, thickness t after hemming is assumed as initial thickness t_0.

The parameter b in the equation of plastic strain energy W can take any value. However, only the one closest to reality can make W minimum. That is,

$$\frac{\mathrm{d}W}{\mathrm{d}b}=0 \tag{14}$$

should be satisfied.

2.3 Defects predictions

2.3.1 Creepage/growing

Creepage/growing is one of the main defects which affects part outline appearance. It is influenced by many factors such as material parameters (e.g., thickness and strength), and process parameters (e.g., flanging die corner radius and pre-hemming path). An illustration of creepage is shown in Fig. 1, and the value can be calculated from the following formula:

$$C=R_f+t/2+Q_2N-(b+A'N), \tag{15}$$

where C is the creepage magnitude, b is the length of $\overline{BO}$, namely the length of major semi-axis, Q_2N and $A'N$ correspond to the lengths of $\overline{Q_2N}$ and $\overline{A'N}$, and $A'N=BN-BA'$.

If the value of C is positive, the outer blank is rolled in creepage occurs. Otherwise, the outer blank is rolled out, and growth occurs.

2.3.2 Maximum plastic strain

Maximum equivalent plastic strain (MEPS) $\bar{\varepsilon}_{max}$ implies the deformation degree and can be used as a criterion of critical crack. If $\bar{\varepsilon}_{max}$ exceeds a critical value, crack may occur. On the outer panel, $\bar{\varepsilon}_{max}$ is located at B_O, and can be calculated by

$$\begin{aligned}\bar{\varepsilon}_{max}&=\bar{\varepsilon}_{f_{out}}+\Delta\bar{\varepsilon}_{Bout}\\&=\frac{2\sqrt{3}}{3}\left|\ln\left(1+\frac{t_0/2}{R_d}\right)\right|+\frac{2\sqrt{3}}{3}\left|\ln\frac{1+t_0/(2\rho_{nB})}{1+t_0/(2R_d)}\right|\\&=\frac{2\sqrt{3}}{3}\ln\left(1+\frac{t_0/2}{\rho_{nB}}\right).\end{aligned} \tag{16}$$

The flow chart of the whole solving process is presented in Fig. 4, which is executed numerically by MATLAB. First, one of the deformation modes is

assumed, as a result of which the relative magnitudes of φ_M and φ_{Q1} are determined. According to the positions of Q_1 and M as shown in Fig. 3, deformation processes and corresponding φ_{k-1} and φ_k of the deformed zone can be determined. Second, b is obtained through Eqs. (7)–(11) and one loop is completed. Then point positions are checked by comparing the magnitudes of φ_M and φ_{Q1}. If they are consistent with the initial assumption, then continue the following calculations. If not, another deformation mode is assumed, and the loop is repeated until the calculated result is consistent with the initial assumption.

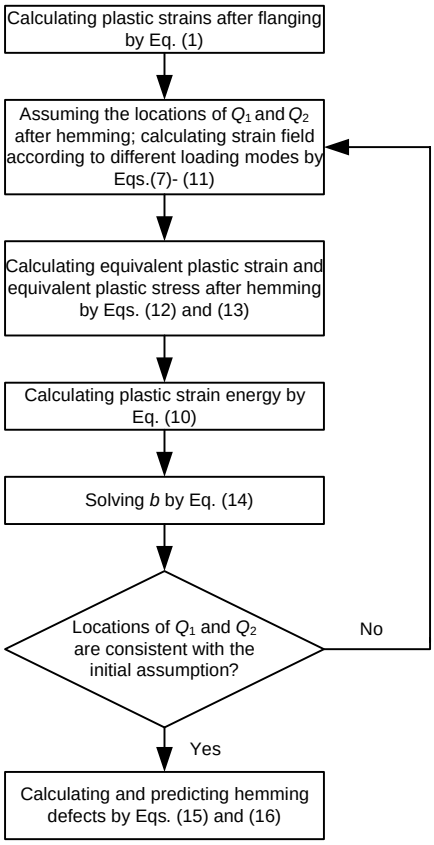

Fig. 4 Flow chart of solving process

3 Results and discussion

3.1 FE simulations and experiments

Experiments were undertaken using a CMT4204 electromechanical testing machine (MTS Systems Corporation Shenzhen Company, China). A drawing with the tool as well as the description of tool is shown in Fig. 5. Creepage and profile with different flanging die corner radii were investigated. Lengths of specimens were measured before and after deformation in order to calculate creepage. 4XC optical microscope (Shanghai Optical Instrument Factory, Shanghai, China) was used to observe and acquire the profile of specimens, and the profile was magnified 50 times.

FE simulation of hemming was carried out by the commercial code ABAQUS standard. Four-node bilinear plane strain quadrilateral element CPE4R is chosen, and the outer panel is divided into six element layers.

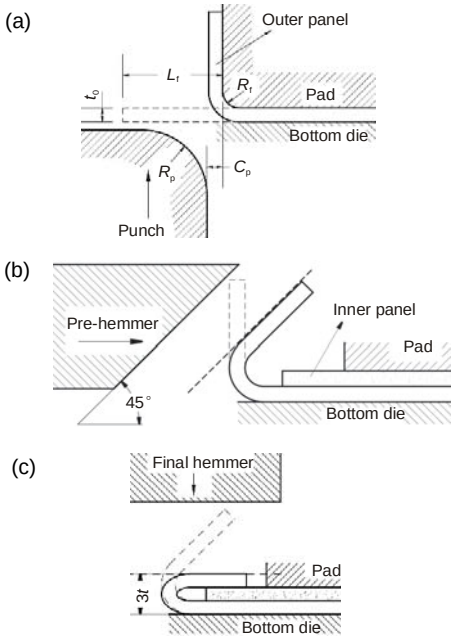

Fig. 5 Hemming procedures

(a) Flanging; (b) Pre-hemming; (c) Final hemming. C_p: punch-die clearance; R_p: punch corner radius

3.2 Comparison of hemming using galvanized steel

To verify the present analytical model, experiments were undertaken. The material used in the experiment is galvanized steel. The geometry and process parameters used in the experiment and FE model are obtained by undertaking uniaxial tension tests and data processing: specimen thickness t_0=0.8 mm for both inner and outer panels, flanging die corner radius R_f=0.5, 1.0, 2.0 mm, flange length L_f=10 mm, punch-die clearance C_p=1.1t_0, and punch

radius R_p=10 mm. Each set of experiments was repeated three times.

The material model in the FE simulation is fitted assuming the plastic region follows the exponential strain hardening law as

$$\begin{cases}\bar{\sigma}=E\bar{\varepsilon}_e,\\ \bar{\sigma}=K(\varepsilon_0+\bar{\varepsilon}_p)^n,\end{cases} \tag{17}$$

where $\bar{\varepsilon}_e$ and $\bar{\varepsilon}_p$ are the equivalent elastic and plastic strains respectively. The material parameters are: Young's modulus E=2.01×10^5 MPa, strength coefficient K=551.34 MPa, strain hardening exponent n=0.278, and prestrain ε_0=0.0031. Other parameters in FE simulation are: Poisson's ratio ν=0.3; yield strength σ_y=143.96 MPa.

The analytical model, however, concerns the strain field at the end of deformation, where the magnitude of strain is much larger. To reduce calculation difficulty, the valid parts of the experiment data with true strain value larger than 0.1 marked out by two vertical dashed lines are fitted by a straight line as shown in Fig. 6, through which the linear rigid plastic hardening model is determined: $\bar{\sigma}=\sigma_0+E_p\bar{\varepsilon}$, where σ_0=268.13 MPa, and E_p=446.88 MPa. Bauschinger effect is neglected and the isotropic hardening model is employed in both FE simulation model and analytical model.

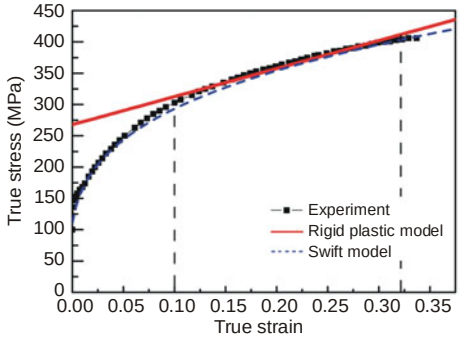

Fig. 6 True stress-strain curve of galvanized steel

Results show that deformation modes are different for each flanging die corner radius. For R_{f1}=0.5 mm and R_{f2}=1 mm, deformation mode is similar to Fig. 3a; for R_{f3}=2 mm, deformation mode is similar to Fig. 3c.

Calculated creepage with different flanging die corner radii is shown in Fig. 7. Results of Zhang (2001)'s model is also shown. When the flanging die corner radius is smaller, strain hardening in the corner becomes more severe, which makes roll-in difficult. As a result, the creepage becomes smaller. It can be seen that all curves have the same trend, that is, smaller flanging die corner radius leads to smaller creepage as shown in Fig. 7. The results of the present analytical model are very close to the experimental results. However, the result of Zhang's model is beyond the error range when flanging die corner radius is 2 mm.

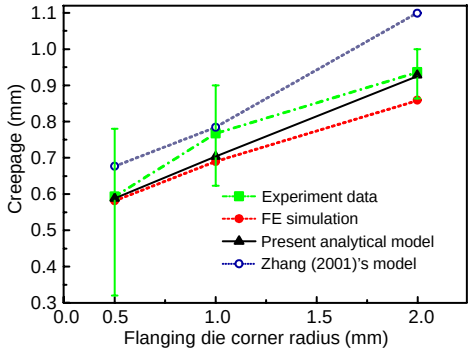

Fig. 7 Relationship between the creepage and flanging die corner radius using galvanized steel

Outer profiles of specimens were obtained by 4XC optical microscope as previously mentioned, which are compared with the results of both FE simulation and the present analytical model. The results show that profiles of different flanging die corner radii are in good agreement with each other. Fig. 8 shows the outer profile with flanging die corner radius R_f=1 mm obtained from the experiment, FE simulation, and analytical model, where x and y are the coordinates of the measured specimen, respectively. The measured curves are shown in Fig. 8a. Vertical line denotes where the inner panel is located, which is used as a reference line. Gaps along the symmetry axis y=0 of three curves are the differences of creepage by three methods. The curves of the experiment are translated to make the left endpoints coincide with the curve of the analytical model as shown in Fig. 8b, so as to compare the corner shapes. Half circle is also shown. It is worth emphasizing that the shape in the corner of the analytical model is very close to that of the experiment. However, the half circle has great difference in shapes. Therefore, using half ellipse to approximate the specimen's neutral layer is more accurate than half circle. Also, major

semi-axis determined by minimum energy method is also effective.

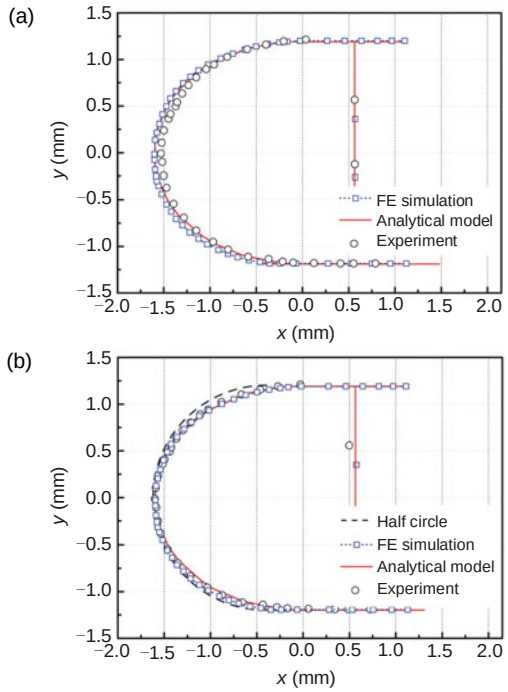

Fig. 8 Outer profile after hemming
(a) Original measured curves; (b) After translation. R_f=1 mm

In the case of galvanized steel, crack did not occur in the outer panel. However, if galvanized steel experienced large deformation before hemming, crack may occur. Also, in high strength steel and aluminum alloy, crack is one of the main defects. As a result, research of MEPS is important.

However, the deformation is mainly concentrated on the corner and it is difficult to measure. Therefore, FE simulations are carried out to obtain the MEPS. The MEPSs with different R_f are given in Fig. 9. Results show that MEPSs by FE simulation

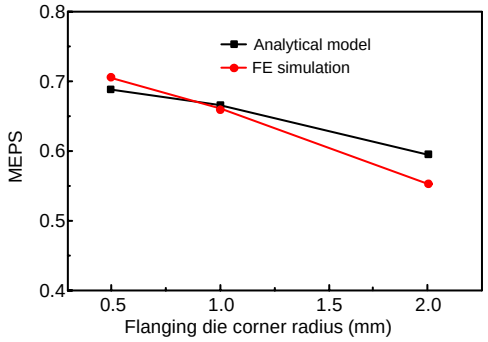

Fig. 9 Relationship between the maximum plastic strains (MEPSs) and flanging die corner radius

change in the same way as those obtained by the analytical model, and are very close to each other in value. This can be explained by their similar calculated outer profiles, that is, similar curvature, which decides the strain field to a large extent.

3.3 Comparison of hemming using aluminum killed draw quality (AKDQ) steel

Livatyali (1998) undertook a systemic research on hemming. For better verification, experimental data of AKDQ steel from Livatyali (1998) is used to verify the present analytical model.

The geometry and process parameters used in the experiment and FE model are as follows (Livatyali, 1998): specimen's thickness t_0=0.84 mm for both inner and outer panels, flanging die corner radius R_f=0.5, 1.0, 2.0 mm, flange length L_f=12 mm, and punch-die clearance C_p=1.1t_0. The material model in the FE simulation is the same as that used in Section 2.2. Material parameters are: Young's modulus E=2.0×10^5 MPa, strength coefficient K=527 MPa, strain hardening exponent n=0.22, and prestrain ε_0=0.0044. Besides, Poisson's ratio v=0.3, and yield stress σ_y=180 MPa.

Corresponding parameters of the material model in the present analytical model are obtained by fitting experimental data from Livatyali (1998) linearly with σ_0=283.8 MPa and E_p=330 MPa.

Creepage of AKDQ steel obtained from experiments, analytical model, and FE simulations were compared in Fig. 10. Results of Zhang (2001)'s model were also adopted. It should be noted that Zhang's model has not taken the material parameters into account. As a result, creepage of Zhang's model maintains constant when material changes from galvanized steel to AKDQ steel.

It can be seen that results of the present analytical model and FE simulation are in good agreement with the experimental results in their error ranges. However, results of Zhang (2001)'s model are out of the range.

As there is no outer profile data in Livatyali (1998), FE simulations are used here for comparison. Fig. 11 presents the specimen's outer profile calculated by the analytical model and FE simulation. Again, specimens with flanging die corner radius R_f=1 mm are used for comparison and shown in Fig. 11a. Maximal gap between the two curves is the

creepage difference between the analytical model and FE simulation. The shape in the corner of the analytical model is very close to that of FE simulation after translating FE simulation curve (Fig. 11b). Accordingly, the assumption of the present analytical model is feasible for AKDQ steel.

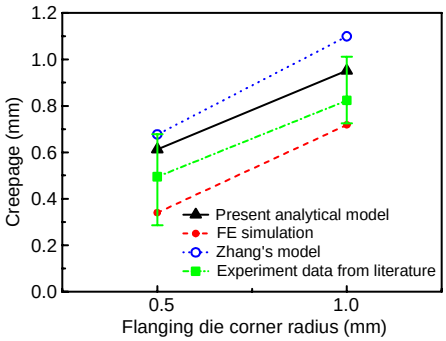

Fig. 10 Relationship between the creepage and flanging die corner radius using aluminum killed draw quality steel

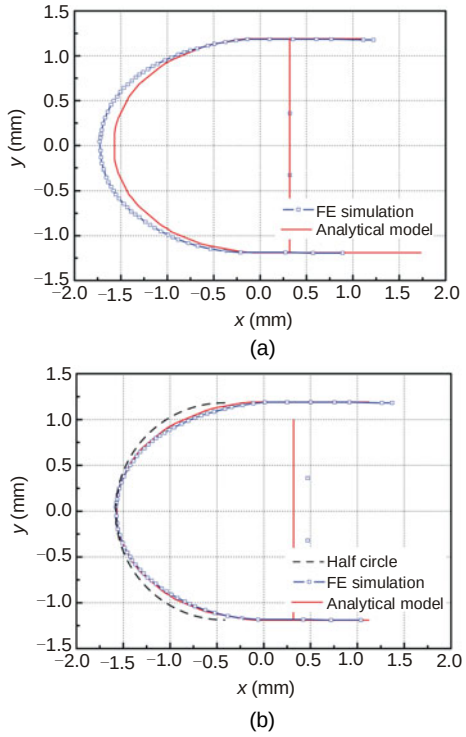

Fig. 11 Outer profile after hemming using aluminum killed draw quality steel

(a) Original measured curves; (b) After translation. R_f=1 mm

3.4 Crack prediction for AA6111-T4

The primary concern for formability of aluminum alloys is surface crack on the outer surface of the corner after final hemming. Lin *et al*. (2009) used AA6111-T4 for hemming with flanging die corner radii of 1.2 and 2.2 mm and blank thickness of 0.92 mm. Material parameters of AA6111-T4 are adopted from Lin *et al*. (2009): Young's modulus E=0.69×10^5 MPa, Poisson's ratio v=0.3, yield stress σ_y=155 MPa, and thickness t_0=0.92 mm. The material model in the FE simulation is

$$\begin{cases}\sigma = E\varepsilon_{\mathrm{e}}, \\ \sigma = K\varepsilon_{\mathrm{p}}{}^{n}, \end{cases} \tag{18}$$

where strength coefficient K=488 MPa, and the strain hardening exponent n=0.232.

Lin *et al*. (2009) obtained the critical equivalent fracture strains of hemming, and also undertook hemming simulation.

MEPS is calculated in the present analytical model. The rigid plastic model is obtained by linearly fitting experimental data from Lin *et al*. (2009), and the corresponding parameters are: σ_0=248.44 MPa; E_p=438.3627 MPa. The isotropic hardening model is employed in both FE simulation model and the analytical model.

Fig. 12 shows the equivalent fracture strains from hemmability tests for AA6111-T4 with samples along rolling and transverse directions from experiments of Lin *et al*. (2009), as well as MEPSs after hemming obtained by the present analytical model. It can be seen that the MEPS exceeds the equivalent fracture strains, which means fracture occurs in the two hemming processes. Lin *et al*. (2009) found that the critical equivalent plastic strain of tested sheet aluminum alloys is independent of the flanging die corner radius. As a result, it can be used as a failure criterion and be implemented into FE simulation. The simulation results for 2D hemming (R_f=2 mm) is illustrated in Fig. 13, and failure occurs at a limiting hemming height corresponding to cracking (LHH) of 3.04 mm, which is larger than three times of the thickness. As a result, crack occurs when hemming has not been completed. That is consistent with the analytical model.

Comparisons of the above results show that the proposed minimum energy method is proved to be valid and practicable. When the material used for hemming is changed, it is very convenient and fast to predict the creepage and crack that may occur after hemming. For a more precise assembly, which means

creepage should be as small as possible, a smaller flanging die corner radius should be chosen. For avoiding crack, in the case of AA6111-T4 with the blank thickness of 0.92 mm, flanging die corner radii of 1.2 and 2.2 mm are too small, and a larger one is suggested. In industry, the choices of hemming dies are limited, which makes process optimization by changing parameters, such as flanging die corner radius, and thickness to avoid defects possible.

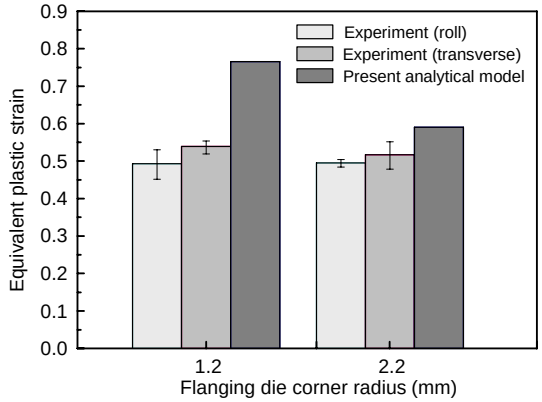

Fig. 12 Relationship between equivalent plastic strain and flanging die corner radius

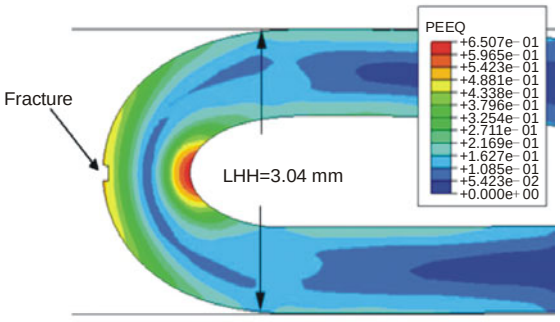

Fig. 13 Failure criterion implementation in 2D hemming simulation (Lin *et al*., 2009)
LHH: limiting hemming heights corresponding to cracking

4 Conclusions

An analytical model for the straight hemming processes, based on the assumption of half ellipse neutral layer and the minimum energy method, is proposed in this paper. Material properties are considered in the present model. Major semi-axis of ellipse neutral layer is obtained, and is applied to calculate creepage, outer profile of specimen, and the maximum plastic strain.

The analytical results are in good agreement with those of FE simulations and experiments. As flanging die corner radii decrease, values of creepage decrease while values of MEPS increase. Profiles obtained from the present analytical model are very close to those from experiments and FE simulations. The model can be used for selecting appropriate material and optimizing process parameters.

References

Buranathiti, T., Cao, J., 2004. An effective analytical model for springback prediction in straight flanging processes. *International Journal of Materials and Product Technology*, **21**(1-3):137-153. [doi:10.1504/IJMPT.2004.004748]

Hu, P., Li, D.Y., Li, Y.X., 2003. Analytical models of stretch and shrink flanging. *International Journal of Machine Tools and Manufacture*, **43**(13):1367-1373. [doi:10.1016/S0890-6955(03)00150-0]

Hu, X., Lin, Z.Q., Li, S.H., Zhao, Y.X., 2010. Fracture limit prediction for roller hemming of aluminum alloy sheet. *Materials and Design*, **31**(3):1410-1416. [doi:10.1016/j.matdes.2009.08.039]

Lin, G.S., Hu, S.J., Cai, W., 2009. Evaluation of formability in bending/hemming of aluminum alloys using plane-strain tensile tests. *Journal of Manufacturing Science and Engineering*, **131**(5):051009-051018. [doi:10.1115/1.3123316]

Livatyali, H., 1998. Computer Aided Process Design of Selected Sheet Metal Bending Process-Flanging & Hemming. PhD Thesis, The Ohio State University, Ohio, USA.

Livatyali, H., Altan, T., 2001. Prediction and elimination of spring back in straight flanging using computer aided design methods. Part 1: experimental investigation. *Journal of Materials Processing Technology*, **117**(1-2):262-268. [doi:10.1016/S0924-0136(01)01164-5]

Livatyali, H., Larris, S.J., 2004. Experimental investigation on forming defects in flat surface-convex edge hemming: roll, recoil and warp. *Journal of Materials Processing Technology*, **153-154**:913-919. [doi:10.1016/j.jmatprotec.2004.04.425]

Livatyali, H., Muderrisoglu, A., Ahmetoglu, M.A., Akgerman, N., Kinzel, G., Altan, T., 2000. Improvement of hem quality by optimising flanging and pre-hemming operations using computer aided die design. *Journal of Materials Processing Technology*, **98**(1):41-52. [doi:10.1016/S0924-0136(99)00304-0]

Livatyali, H., Wu, H.C., Altan, T., 2002. Prediction and elimination of springback in straight flanging using computer-aided design methods Part 2: FEM predictions and tool design. *Journal of Materials Processing*

Technology, **120**(1-3):348-354. [doi:10.1016/S0924-0136(01)01161-X]

Livatyali, H., Laxhuber, T., Altan, T., 2004. Experimental investigation of forming defects in flat surface-convex edge hemming. *Journal of Materials Processing Technology*, **146**(1):20-27. [doi:10.1016/S0924-0136(03)00840-9]

Maoût, N.L., Thuillier, S., Manach, P.Y., 2009. Aluminum alloy damage evolution for different strain paths-application to hemming process. *Engineering Fracture Mechanics*, **76**(9):1202-1214. [doi:10.1016/j.engfracmech.2009.01.018]

Muderrisoglu, A., Murata, M., Ahmetoglu, M.A., Kinzel, G., Altan, T., 1996. Bending, flanging, and hemming of aluminum sheet-an experimental study. *Journal of Materials Processing Technology*, **59**(1-2):10-17. [doi:10.1016/0924-0136(96)02281-9]

Song, N., Qian, D., Cao, J., Liu, W.K., Li, S.F., 2001. Effective models for prediction of springback in flanging. *Journal of Engineering Materials and Technology*, **123**(4):456-461. [doi:10.1115/1.1395019]

Wang, C.T., Kinzel, G., Altan, T., 1994. Wrinkling criterion for an anisotropic sheet with compound curvatures in sheet forming. *International Journal of Mechanical Sciences*, **36**(10):945-960. [doi:10.1016/0020-7403(94)90056-6]

Wang, C.T., Kinzel, G., Altan, T., 1995. Failure and wrinkling criteria and mathematical modeling of shrink and stretch flanging operations in sheet metal forming. *Journal of Materials Processing Technology*, **53**(3-4):759-780. [doi:10.1016/0924-0136(94)01766-T]

Wang, N.M., Wenner, M.L., 1974. An analytical and experimental study of stretch flanging. *International Journal of Mechanical Sciences*, **16**(2):137-143. [doi:10.1016/0020-7403(74)90082-4]

Zhang, G.H., 2001. Analysis and Optimization of Sheet Metal Flanging and Hemming Processes. PhD Thesis, The University of Michigan, Michigan, USA.

Zhang, G.H., Hao, H.Q., Wu, X., Hu, S.J., Harper, K., Faitel, W., 2000. An experimental investigation of curved surface-straight edge hemming. *Journal of Manufacturing Processes*, **2**(4):241-246. [doi:10.1016/S1526-6125(00)70025-9]

Zhang, G.H., Wu, X., Hu, S.J., 2001. A study on fundamental mechanisms of warp and recoil in hemming. *Journal of Engineering Materials and Technology*, **123**(4):436-441. [doi:10.1115/1.1396348]

Zhang, G.H., Hu, S.J., Wu, X., 2003. Numerical analysis and optimization of hemming processes. *Journal of Manufacturing Processes*, **5**(1):87-96. [doi:10.1016/S1526-6125(03)70044-9]